CrossMark

Two-dimensional tungsten photonic crystal selective emitter: effects of geometrical parameters and temperature

Ali Rostamnejadi[1] · Meysam Daneshvar[1]

Abstract

In this paper, we have studied the effects of structural parameters and temperature on the emissivity of a square array of cylindrical nano/microcavities on tungsten slab by finite difference time domain method. It has been shown that the physical nature of the emissivity enhancement depends on the structural parameters of the nano/microcavities. In the case of narrow and shallow nanocavities with radius $r \leq 150$ nm and depth $d \leq 150$ nm; the emissivity has the same behavior as that of flat tungsten. Thermally excited surface plasmon polaritons cause a sharp peak in the emissivity of nanocavities with $150 \leq d \leq 250$ nm and $150 \leq r \leq 350$ nm at wavelength in the order of periodicity, $\lambda \sim a$. In the case of wide and deep microcavities with $r \geq 350$ nm and $d \geq 250$ nm; there are anomalous peaks in the emissivity which are well matched with the modified resonant wavelengths of a microcavity. At wavelengths shorter than periodicity, the Bragg diffraction from the surface of periodic microcavities reduces the emissivity. The obtained results show that to have a favorable selective thermal emitter from 2D W nano/microcavities with emission efficiency more than 90%, the periodicity should be as small as possible, the cavity depth should be large enough and its radius should be selected according to the working temperature.

1 Introduction

In the past decade, the controlled light–matter interaction by periodic nano/microstructures has attained a lot of attention because of the complex physics and widespread applications [1–7]. It is well known that electromagnetic wave propagation, scattering and radiation can be controlled by periodic nano/microstructures with dimensions in the order of light wavelength [2, 3, 8–11]. Highly selective absorbers and thermal emitters are critical elements in the solid state converting energy systems such as thermophotovoltaic (TPV), solar cells and solar absorbers [5, 12, 13]. In a TPV system, the radiated thermal energy from a high-temperature selective emitter is converted into electricity by a photovoltaic (PV) cell. A proper selective emitter should be designed to radiate electromagnetic waves with energy mainly higher than the electronic band gap of the PV cell.

Metallic photonic crystals have promising potential to be used as selective thermal emitter and absorber [5, 14–16].

Using such structures allows achieving near-blackbody emissivity in a desired region and low emissivity like that of flat metal at longer wavelengths [17–20]. Recently, photonic crystals of different materials such as W, Ta, W–Ta alloys, and VO_2 have been proposed as selective thermal emitter in TPV systems [4, 17, 21–25]. Due to the high-temperature stability and its natural selective emissivity, different nano/microstructures of W have been considered to be used in converting thermal energy systems [26–31]. The thermally excited radiation of nano/microcavities depends strongly on the geometrical parameters of the periodic structures [29, 32, 33]. Therefore, to have a favorable selective thermal emitter based on metallic photonic crystals, it is necessary to study the effects of structural parameters on emissivity at high temperatures.

In this paper, the effects of temperature and geometrical parameters on thermal emission properties of 2D W photonic crystal slab (PhCS) have been investigated by finite difference time domain (FDTD) method. The obtained results show large enhancement with remarkable selectivity in the thermal emission spectra of W PhCS relative to that of flat W. The ability of W PhC to emit at desired wavelengths is described based on the coupling between thermally excited radiation with the resonance modes inside of the nano/microcavities, thermally excited SPP and Bragg diffraction modes from the surface of

✉ Ali Rostamnejadi
 ali@ph.iut.ac.ir

1 Department of Electroceramic and Electrical Engineering, Malek Ashtar University of Technology, Shahin Shahr, Isfahan, Iran

periodic nano/microcavities. The resonance wavelengths of an optical microcavity have been modified by considering the effect of skin depth, which are well matched with the simulated results. The physical nature of the observed peaks in the emissivity is quantified by introducing aspect ratio and aperture ratio of a nano/microcavity.

2 Simulation method

In this paper, FDTD method has been employed to study the optical properties and spectral thermal emission of the photonic crystal slabs [34]. The numerical simulations have been carried out by MEEP, a freely available package developed at MIT [35]. The PhCS consists of a square array of cylindrical air-filled nano/microcavities on tungsten with radius r and depth d. A schematic diagram of the PhCS and a computational unit cell are shown in Fig. 1. A normally incident Gaussian pulse temporally illuminates the photonic crystal slab. The electric field of the incident wave is perpendicular to the cavity axis. The passing fields through the flux planes on the front and backside of the slab are recorded. The Poynting vector has been calculated at each frequency by Fourier-transform integration of the electric and magnetic fields, which leads to the total reflected and transmitted power [1].

The spectral thermal emissivity is obtained from the calculated absorbance via Kirchhoff's law [21, 26]. Based on this law, at thermal equilibrium, the emissivity $\varepsilon(\theta,\lambda)$ of a body at any incidence angle θ and wavelength λ is equal to its absorbance, $\alpha(\theta,\lambda)$. In our case, the thickness of the metallic substrate is much larger than the skin depth of W, therefore, the transmission is zero and the spectral emissivity is:

$$\varepsilon(\theta, \lambda) = \alpha(\theta, \lambda) = 1 - \rho(\theta, \lambda), \tag{1}$$
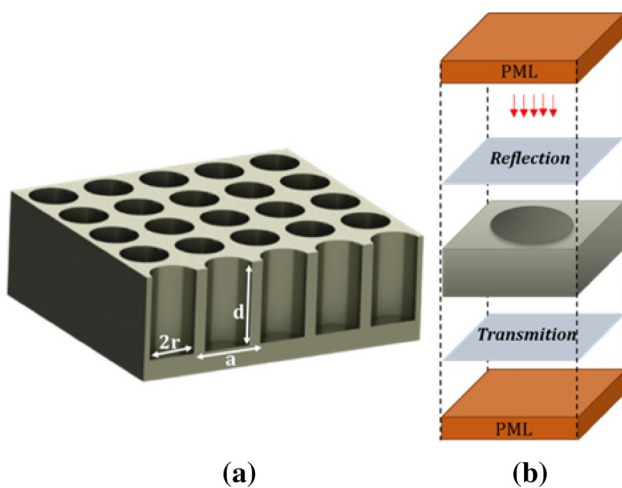
Fig. 1 **a** 2D W PhCS with period a, depth d and radius r. **b** Computational unit cell for calculating the optical spectrum

where $\rho(\theta,\lambda)$ is the reflectance. The Drude–Lorentz model could be used to model the complex permittivity of a metallic material as:

$$\varepsilon(\omega) = \varepsilon_{\mathrm{D}}(\omega) + \varepsilon_{\mathrm{L}}(\omega) = 1 - \frac{f_1 \omega_{\mathrm{p}}^2}{(\omega^2 + i\gamma_1 \omega)} + \sum_{n=2} \frac{f_n \omega_{\mathrm{p}}^2}{\omega_n^2 - \omega^2 - i\gamma_n \omega}, \tag{2}$$

In this equation, ω_{p} is plasma frequency and ω_n, f_n and γ_n are the resonance frequency, oscillator strength, and damping coefficient of the nth oscillator, respectively. The Drude term shows the free electron contribution and the Lorentz term reveals the interband transition contributions. By choosing a length scale of 1 μm and selecting some new parameters as $\varepsilon_{\infty} = \hat{\varepsilon}(\omega \to \infty) = 1$, $\sigma_n = \frac{f_n \omega_{\mathrm{p}}^2}{\omega_n^2}$ and $\omega_1 = 0$, the permittivity takes the following form:

$$\hat{\varepsilon}(\omega) = \varepsilon_{\infty} + \sum_n \frac{\sigma_n \omega_n^2}{\omega_n^2 - \omega^2 + i\gamma_n \omega}. \tag{3}$$

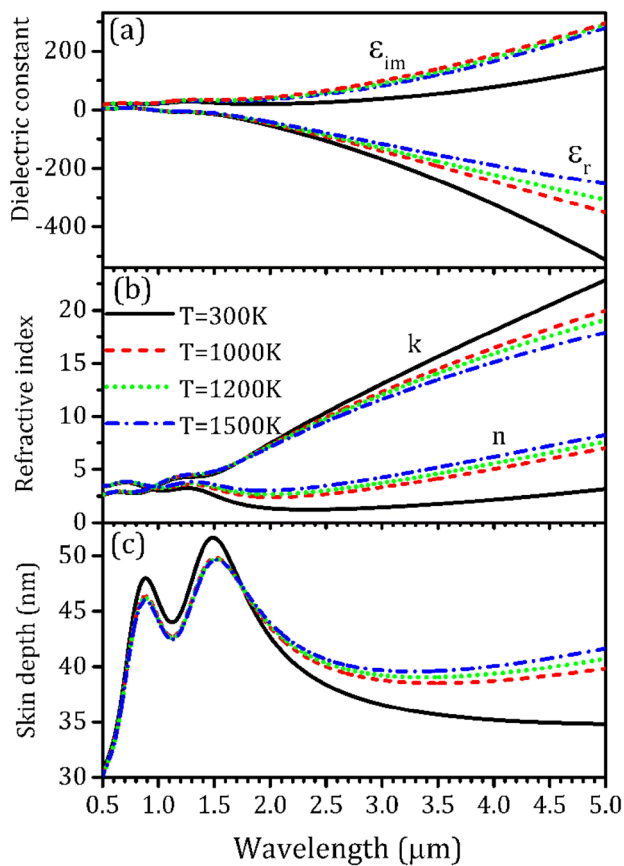The real and imaginary parts of the permittivity are given as follows:

$$\mathrm{Re}\,\hat{\varepsilon}(\omega) = \varepsilon_{\infty} + \sum_n \frac{\sigma_n \omega_n^2 (\omega_n^2 - \omega^2)}{(\omega_n^2 - \omega^2)^2 + (\gamma_n \omega)^2}, \tag{4}$$

$$\mathrm{Im}\,\hat{\varepsilon}(\omega) = \sum_n \frac{\sigma_n \omega_n^2 \gamma_n \omega}{(\omega_n^2 - \omega^2)^2 + (\gamma_n \omega)^2}. \tag{5}$$

We have used the reported experimental data of W in Ref [36] to obtain the Drude–Lorentz parameters. The high-temperature dielectric constants are usually determined by fitting the experimental data of the bulk tungsten to the Drude–Lorentz model. In the case of lacking experimental data, a semi-empirical model could be used to obtain the permittivity over a wide range of temperatures. Based on this model, the damping coefficient $\gamma_1(T)$ at temperature T is related to the room temperature value by following equation [37, 38]:

$$\gamma_1(T) = \gamma_1(T_0)\left(\frac{T}{T_0}\right)^{\alpha}, \tag{6}$$

Comparing experimental data of tungsten with the above model leads to $\alpha = 0.85$ [37]. Considering this model, the relative permittivity, refractive index and skin depth of W at different temperatures are calculated, which are shown in Fig. 2. The results show that by increasing temperature, the refractive index increases and the extinction coefficient decreases; leading to a large increase in the skin depth of W at wavelengths longer than 2 μm. In addition the real part of
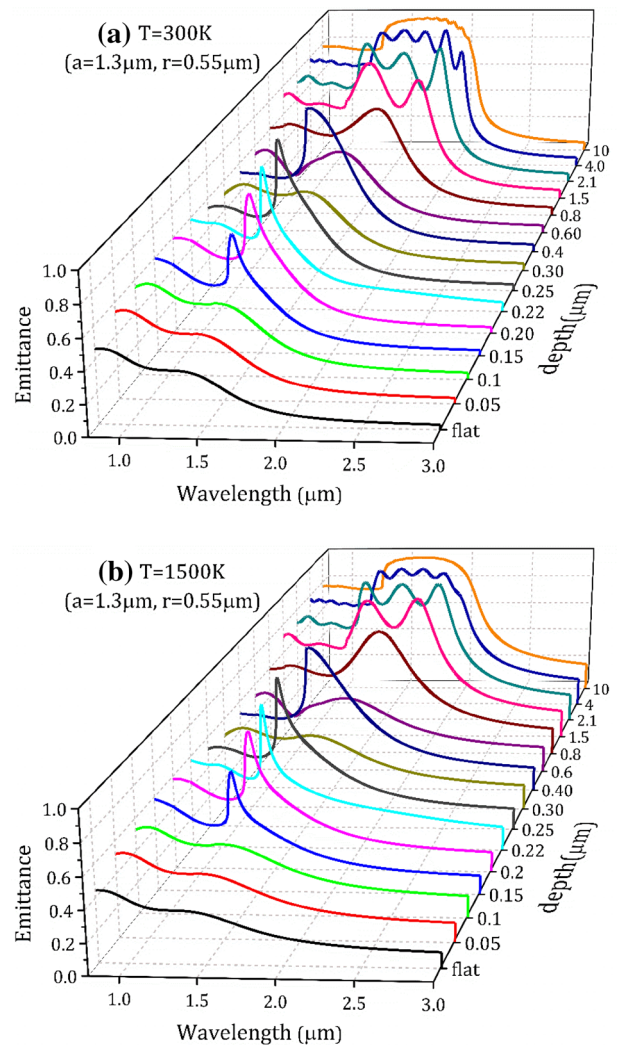
Fig. 2 **a** Real and imaginary parts of permittivity, **b** real and imaginary parts of Refractive Index and **c** skin depth of W at different high temperatures

Fig. 3 Normal emissivity spectra of 2D W PhCS versus wavelength for different cavity depths ($a = 1.30$ μm; $r = 0.55$ μm). **a** $T = 300$ K and **b** $T = 1500$ K

dielectric constant becomes less negative, which decreases the reflectivity of *W* at longer wavelengths.

3 Results and discussions

It is well known that the thermal emission properties of a material depend on its microscopic properties as well as on its surface microstructure [29, 32, 33, 39]. By producing roughness on the surface of a material, its emissivity increases in the whole wavelength region [32]. In the case of periodic microstructures, with structural parameters comparable to the optical wavelengths, anomalous behaviors occur in the emissivity. Here, we have studied the effects of structural parameter on the thermal emission spectrum of 2D W PhCS. The normal spectral emissivities of flat W and 2D W PhCS at 300 and 1500 K, for different cavity depths are shown in Fig. 3. In the case of shallow nanocavities with depth lower than 100 nm, the emissivity is the same as that of flat W. By increasing the cavity depth from 150 to 250 nm, a sharp peak appears at wavelength $\lambda \sim a$. For

deeper cavities with $d \geq 300$ nm, a large enhancement is observed in the emissivity in comparison to that of flat *W* in the wavelengths $\lambda \leq 2$ μm. At wavelengths longer than 2 μm, the emissivity sharply decreases and reaches the value of flat W. Figure 3 also shows that there are some peaks in the spectrum at wavelengths below the cutoff, which their number increases by increasing the cavity depth. For cavity depths greater than 4 μm, the emissivity reaches the maximum value, near unity, in the wavelength range of $a \leq \lambda \leq \lambda_{\text{cutoff}}$.

Emissivity spectra variation versus radius at two different temperatures $T = 300$ and 1500 K is depicted in Fig. 4, where the depth and period are fixed at 3.00 and 1.30 μm, respectively. It can be seen that emissivity increases with increasing radius relative to that of flat W in the whole wavelength range, which is related to the
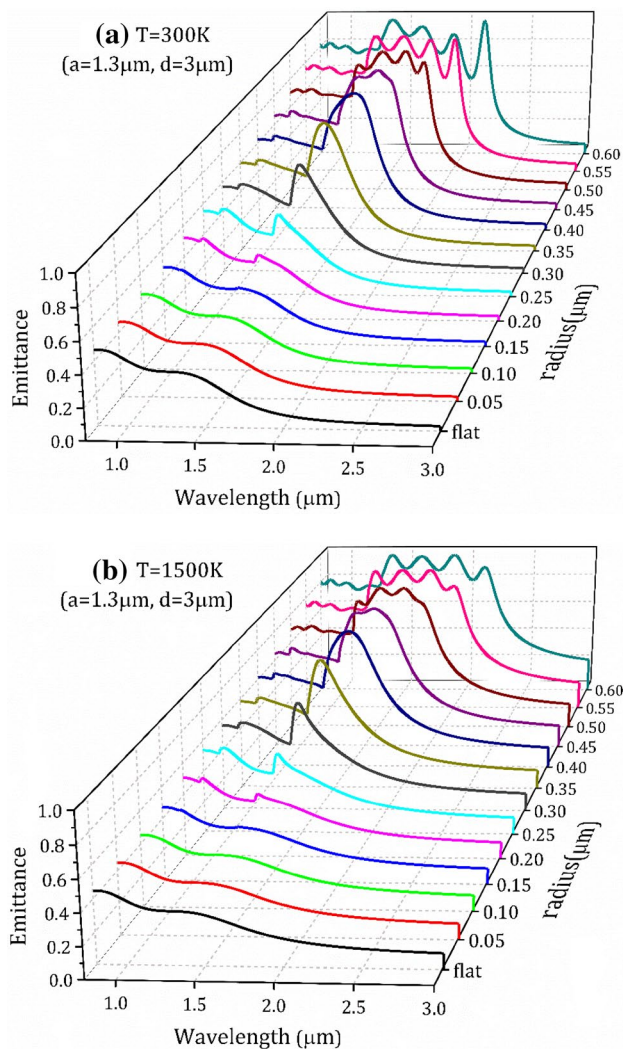
Fig. 4 Normal emittance of 2D W PhCS at different radii ($a = 1.30$ μm; $d = 3$ μm). **a** $T = 300$ K and **b** $T = 1500$ K

surface roughness increasing in the nano/microcavities [40]. For small radiuses $r = 50$ and 100 nm, the emissivity has the same value and trend as that of flat W. By increasing the radius from 150 to 350 nm, a sharp peak appears in the emissivity at wavelength $\lambda \sim a$, near to the first diffracting mode of periodic surface. The more increase in the cavity radius leads to large enhancement and remarkable selectivity with some resonance peaks in the emissivity spectra. It is apparent from Figs. 3 and 4 that the calculated emissivity at 1500 K is slightly greater than the corresponding value at 300 K, especially in the wavelengths longer than the cutoff wavelength. This is due to the increase of electron–phonon interaction by increasing the temperature. In our calculations, we have neglected the length change due to the low thermal expansion coefficient (α) of W. Below 2500 K, α of W

is less than 6 μm m^{-1} K^{-1} [41, 42], leading to a relative length change less than 1%. Therefore, in practice thermal expansion does not affect the emissivity of photonic crystal of W in the optical wavelengths [1].

Some phenomena could be proposed to describe the physical nature of the observed enhancement and selectivity in the emissivity of structured surfaces. The anomalous behavior in the emissivity at wavelengths below the cutoff relates to the cavity and photonic band gap effects. The coupling between thermally excited electromagnetic waves with the resonance modes inside of the cavity is one of the main mechanisms of emissivity enhancement. The resonance wavelengths of an ideal metallic microcavity depend on its structural parameters [43]. Figure 5 shows the position of the observed peaks by depth and radius of the nano/microcavity. It is clear from the figure that the positions of the peaks are shifted to the longer wavelengths with increasing the depth and radius of cavity monotonically, which are more sensitive in respect to the radius variation. The resonance wavelengths of a one open-end cylindrical cavity with radius r and depth d could be approximated by the resonance wavelengths of a corresponding enclosed one in which only the odd number of quarter wavelengths could take place along the cavity [3, 6, 44];

$$(\lambda_r)_{\mathrm{TM}_{mnp}} = \frac{2\pi c \sqrt{\varepsilon\mu}}{\sqrt{\left(\frac{\chi_{mn}}{r}\right)^2 + \left(\frac{p\pi}{2d}\right)^2}}, \tag{7}$$

$$(\lambda_r)_{\mathrm{TE}_{mnp}} = \frac{2\pi c \sqrt{\varepsilon\mu}}{\sqrt{\left(\frac{\chi'_{mn}}{r}\right)^2 + \left(\frac{p\pi}{2d}\right)^2}}, p = 1, 3, 5, \dots. \tag{8}$$

Here m and n are integers, χ_{mn} and χ'_{mn} are the nth root of the mth order Bessel function and its derivative, μ and ε are permeability and permittivity of the material filling the cavity, respectively. Equations (7) and (8) show that cutoff wavelength (the highest resonant wavelength) of TE and TM modes are TM$_{010}$ and TE$_{111}$, respectively. It is clear from Fig. 5 that there is a large difference (about 12%) between the resonance wavelength obtained from the FDTD method and the corresponding values estimated from the ideal metallic cavity. Such increase in the resonance wavelength is due to the finite conductivity and non-zero skin depth of tungsten metal [6, 45–47]. To modify the resonance wavelengths of a one open-end cylindrical cavity, we assumed that the boundaries of the metallic cavity are shifted into the metal with a length in order of skin depth. Therefore, the modified TE resonance wavelengths of a cylindrical cavity are determined by adding the skin depth to the radius and depth of the cavity as:

Fig. 5 Simulated, estimated and modified resonant peaks of 2D W PhC as a function of cavity depth (left) and cavity radius (right) at $T = 300$ K
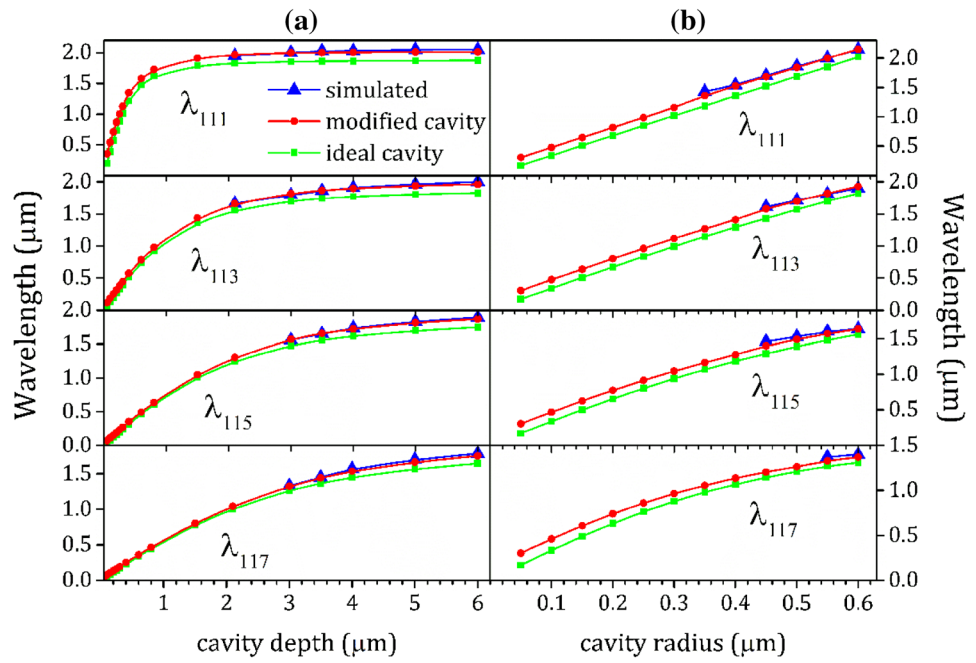
In this equation δ is the skin depth of the bulk metal at the resonant wavelength. Figure 5 shows the modified resonance wavelengths of 2D W PhCS versus radius and depth.

$$(\lambda_r)_{\mathrm{TE}_{mnp}} = \frac{2\pi c \sqrt{\varepsilon \mu}}{\sqrt{\left(\frac{\chi'_{mn}}{(r+\delta(\lambda))}\right)^2 + \left(\frac{p\pi}{2(d+\delta(\lambda))}\right)^2}}, p = 1, 3, 5, 7, \dots. \tag{9}$$

The results show that the modified TE resonance wavelengths are in good agreement with the values obtained from the FDTD simulation, with maximum deviation less than 3%. Such calculations have also been carried out for the TM modes but the observed peaks are not consistent with the resonant wavelengths of this mode.

The positions of the simulated peaks in the emissivity at 300 and 1500 K for various radius and depth are given in Table 1. It could be found from Table 1 that the resonance wavelengths are slightly decreased by changing temperature from 300 to 1500 K, with maximum variation less than 3%. As it can be seen from Fig. 2, this variation could be attributed to the change of skin depth at higher temperatures. In periodic nano/microstructures, the photonic band gap effect could be attributed to the emissivity enhancement. This effect suppresses the thermal radiation inside the photonic crystal in the band gap region and increases the density of state in the near band gap edges [2]. The increasing in the density of state could increase the number of excited modes in direction normal to the photonic crystal.

Table 1 Comparing the peak position in the emissivity of 2D W PhCS for different structural parameters at $T_1 = 300$ K and $T_2 = 1500$ K

2D tungsten photonic crystal ($a = 1.3$)

PhC characterizes		λ_1 (µm)		λ_2 (µm)		λ_3 (µm)	
r	d	T_1	T_2	T_1	T_2	T_1	T_2
0.45	3	1.70	1.67	1.61	1.57	1.47	1.44
0.50		1.86	1.84	1.71	1.69	1.53	1.51
0.55		2.00	1.99	1.81	1.80	1.60	1.58
0.60		2.15	2.14	1.90	1.89	1.64	1.63
0.55	1.5	1.87	1.86	1.48	1.47	–	–
	2.1	1.95	1.93	1.66	1.65	1.38	1.36
	4.0	2.04	2.02	1.91	1.89	1.74	1.72
	10	–	–	1.89	1.86	1.82	1.80

The SPP formation at the interface of dielectric and metallic materials can be also attributed to the emissivity enhancement in periodic nano/microstructures. The surface plasmons can be excited when the real part of dielectric constant of the metal is negative. Figure 2a shows that this could be satisfied for W at wavelength longer than $\lambda \sim 0.95$ μm. The diffraction grating theory implies that anomalous absorption occurs due to the excitation of surface waves through the periodicity of gratings. In the case of 2D square lattice gratings, the wavelength of normally excited SPP, λ_{SPP}, is given by [48];

$$\lambda_{SPP}(m,n) = \frac{a}{\sqrt{m^2 + n^2}} \sqrt{\frac{\varepsilon}{1+\varepsilon}}, \tag{10}$$

where m and n are integer numbers indicating the diffraction order, a is lattice constant and ε is the metal's dielectric constant. A 2D periodic array of nano/microcavities can be regarded as a 2D grating. Figure 3 shows that in the case of shallow nanocavities with fixed $r = 550$ nm and depth $150 \leq d \leq 250$ nm, the anomalous absorption peak around $\lambda \sim 1.3$ μm is consistent with $\lambda_{SPP}(1,0)$ and $\lambda_{SPP}(0,1)$ of SPP modes, rather than the resonance modes of the nanocavity. Such behavior is also observed in the emissivity of nanocavities with radius $150 \leq r \leq 350$ nm at fixed depth $d = 3$ μm. In the case of deeper and wider microcavities with $d \geq 250$ nm and $r \geq 350$ nm, the absorption peak is broadened and it is well matched with the cavity-resonant mode. The SPP and cavity-resonant modes could be distinguished by defining aperture ratio and aspect ratio of a cavity. In the case of radius variation, aperture ratio is a good measure to determine the dominant mode, which is defined as the ratio of the occupied surface by a cavity to the surface of a unit cell, $\alpha = \frac{\pi r^2}{a^2} \times 100$ [48]. The obtained results show that in the case of nanocavities with $\alpha \leq 2\%$, the emissivity has the same behavior as that of flat W and there is no any absorbing peak corresponding to the excited SPP or resonant modes of the nanocavity. For $4 \leq \alpha \leq 125$, the thermally excited SPP modes and for $\alpha \geq 22\%$, the microcavity-resonant modes are dominant. In the case of depth variation, aspect ratio of a cavity $\left(\beta = \frac{d}{r} \times 100\right)$ is used to determine the dominant mode.

The obtained results show that for shallow nanocavities with low aspect ratio of $\beta \leq 18\%$, there is no any peak in the emissivity spectra corresponding to the thermally excited SPP or cavity resonant modes. For the aspect ratio $27 \leq \beta \leq 40\%$, the sharp peak is consistent to the thermally excited SPP modes. In the case of deeper microcavities with $\beta \geq 45\%$ the resonant modes inside of microcavities are dominant.

At wavelengths shorter than periodicity, the emissivity variation could be related to the diffracted modes from the
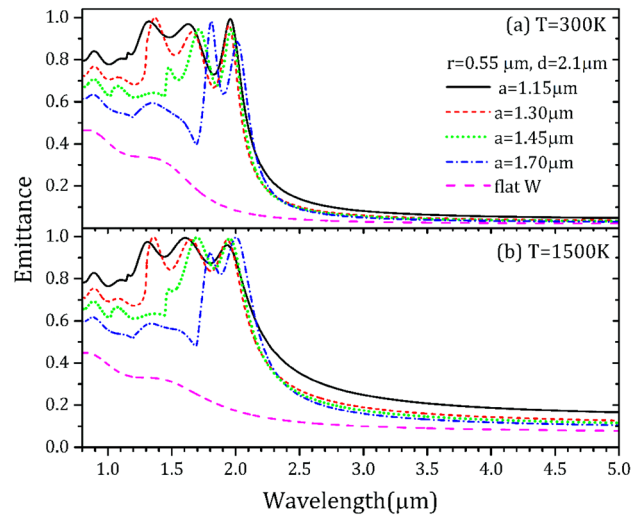
Fig. 6 Normal emittance of 2D W PhCS versus periodicity at fixed $r = 0.55$ μm; $d = 2.10$ μm. **a** $T = 300$ K, **b** $T = 1500$ K

surface of the periodic nano/microcavities. The effect of the lattice constant on the normal emissivity of 2D W PhCS for fixed $r = 0.55$ μm and $d = 2.1$ μm, is shown in Fig. 6. This figure shows that with increasing periodicity, the emissivity decreases significantly in the wavelengths $\lambda \leq a$. The grating equation can be used to explain it as [6];

$$a(\sin \theta_i + \sin \theta_m) = m\lambda, m = \pm 1, \pm 2, \pm 3, ..., \tag{11}$$

In this equation a is the periodicity, m is diffraction order, λ is optical wavelength in free space, θ_i and θ_m are incident and diffraction angles, respectively. In the case of a normally incident wave, the onset of diffraction occurs at $\theta_m = 90$ with corresponding wavelength of $m\lambda = a$, which means that only optical waves with wavelength $\lambda \leq a$ could couple to the diffractive modes. Therefore, by increasing the periodicity, threshold of diffracting modes changes to the longer wavelengths; leading to a decrease in total emittance below the cutoff.

The capability of 2D W PhCS as a high-temperature selective emitter has been studied here. The spectral radiance $I_{PhC}(\lambda, T)$ of a PhC with emittance $\varepsilon_{PhC}(\lambda, T)$ is given by;

$$I_{PhC}(\lambda, T) = I_{BB}(\lambda, T)\varepsilon_{PhC}(\lambda, T) = \frac{2hc^2}{\lambda^5 \left(\exp\left[\frac{hc}{\lambda k_B T}\right] - 1\right)} \varepsilon_{PhC}(\lambda, T), \tag{12}$$

where $I_{BB}(\lambda, T)$ is the blackbody radiation given by Planck's law. The emission efficiency η_e, which measures the amount of radiation below the cutoff wavelength relative to a blackbody with the same conditions is calculated as [49]:

$$\eta_e = \frac{P_{useful}^{PhC}}{P_{useful}^{BB}} = \frac{\int_0^{\lambda_c} d\lambda \varepsilon_{PhC}(\lambda, T) I_{BB}(\lambda, T)}{\int_0^{\lambda_c} d\lambda I_{BB}(\lambda, T)}, \tag{13}$$

Table 2 The effect of period and cavity depth on the emission and conversion efficiencies of W PhC

| $r=0.55$, $d=10$ (µm)			$r=0.55$, $a=1.15$ (µm)		
a (µm)	η_e (%)	η_c (%)	d (µm)	η_e (%)	η_c (%)
1.15	93.1	64.2	1.5	88.1	54.8
1.2	92.5	67	2	92.1	62
1.3	90	68.8	3	92.2	62.3
1.45	84.1	68.8	5	92.9	62.4
1.6	76.5	67.4	6	93.1	62.4
1.7	70.6	65.8	10	93.1	64.2

where λ_c is the cutoff wavelength of the cavity and P_{useful} is the useful radiated power by the emitter. The conversion efficiency, η_c, quantifies the selectivity of an emitter and is defined as the useful radiated power below λ_c relative to the total power as [25];

$$\eta_c = \frac{P_{useful}^{PhC}}{P_{total}^{PhC}} = \frac{\int_0^{\lambda_c} \mathrm{d}\lambda \varepsilon_{PhC}(\lambda, T) I_{BB}(\lambda, T)}{\int_0^{\infty} \mathrm{d}\lambda \varepsilon_{PhC}(\lambda, T) I_{BB}(\lambda, T)}, \tag{14}$$

To optimize the geometry of W PhCS as an efficient emitter, the emission and conversion efficiencies versus period and cavity depth at $T=1500$ K have been calculated and the results are shown in Table 2.

It can be seen from Table 2 that by increasing the cavity depth from 1.5 to 10 µm, both emission and conversion efficiencies are increased. As mentioned above, by increasing the cavity depth, the number of the cavity-resonant modes below the cutoff increases and as a result the useful emittance of PhC cavity increases. For fixed $r=0.55$ µm and $d=10$ µm, with increasing periodicity from 1.15 to 1.7 µm, the emission efficiency decreases monotonically from 93 to 71%, but the conversion efficiency fluctuates between 64–69%. The calculated efficiencies reveal that to have a favorable thermal emitter of 2D W PhCS, the cavity should be deep enough and the periodicity should be as small as possible. Cavity radius determines the cutoff wavelength of PhC emittance, which should be matched to the PV cell band gap.

Based on the results, optimized 2D W PhCS emitters at different temperatures, corresponding to the cutoff wavelengths of the emitters and PV cell band gaps have been designed. The spectral emissions of the optimized emitters are shown in Fig. 7 and the calculated efficiencies and related operating temperatures are given in Table 3. The obtained results show that the designed emitters based on 2D W PhCS have the same spectral emissions as that of the blackbody below the cutoff wavelengths.
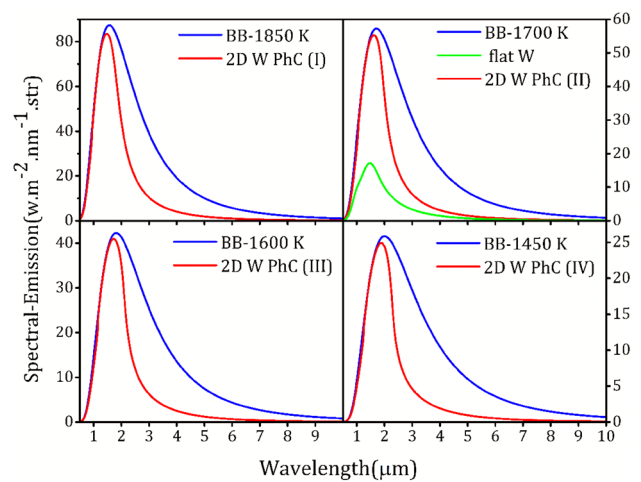
Fig. 7 Spectral emission of designed 2D W PhCS emitters with certain cutoff wavelengths. (1): $a=0.95$, $r=0.45$, (2): $a=1.05$, $r=0.5$, (3): $a=1.15$, $r=0.55$, (4): $a=1.25$, $r=0.6$. For all cases $d=10$ and the values are in µm

Table 3 Optimized structural parameters of the emitters with their emission and conversion efficiencies

Parameters (µm)	λ_c (µm)	T (K)	η_e (%)	η_c (%)
$a=0.95$, $r=0.45$, $d=10$	1.95	1850	91	68
$a=1.05$, $r=0.50$, $d=10$	2.00	1700	93	65
$a=1.15$, $r=0.55$, $d=10$	2.15	1600	92	69
$a=1.25$, $r=0.60$, $d=10$	2.30	1450	92	68

4 Conclusion

In this research, the effects of geometrical parameters and temperature on thermal emission properties of 2D W PhCS have been investigated by FDTD method. The obtained results show large enhancement and remarkable selectivity in the emissivity of the PhCS relative to that of flat W. At wavelength shorter than the periodicity, the emissivity is decreased due to the Bragg diffraction of the electromagnetic wave from the surface of photonic crystal. In the case of shallow and narrow nanocavities, SPP excitation has a sharp peak at $\lambda \approx a$ in the emissivity which is disappeared in deeper and wider microcavities. At wavelengths longer than periodicity, the enhancement is mainly related to the coupling between thermal emission modes with the resonance modes inside the microcavity. The positions of the resonance modes are well matched with the modified resonance wavelengths of the microcavity. By increasing temperature, the emissivity increases slightly at wavelengths longer than the cutoff, but the positions of the resonance wavelengths are not changed significantly. Optimized thermal emitters of W microcavities with emission efficiency more than 90% have been designed,

which are suited for high-temperature thermal energy conversion in the thermophotovoltaic systems.

References

1. Y.X. Yeng, M. Ghebrebrhan, P. Bermel, W.R. Chan, J.D. Joannopoulos, M. Soljačić, I. Celanovic, Proc. Natl. Acad. Sci. USA **109**, 2280 (2012)
2. J.D. Joannopoulos, S.G. Johnson, J.N. Winn, R.D. Meade, Photonic crystals: molding the flow of light (Princeton university press, Princeton, 2011)
3. V. Rinnerbauer, S. Ndao, Y.X. Yeng, W.R. Chan, J.J. Senkevich, J.D. Joannopoulos, M. Soljacic, I. Celanovic, Energy Environ. Sci. **5**, 8815 (2012)
4. V. Rinnerbauer, S. Ndao, Y.X. Yeng, J.J. Senkevich, K.F. Jensen, J.D. Joannopoulos, M. Soljačić, I. Celanovic, R.D. Geil, J. Vac. Sci. Technol. B **31**, 011802 (2013)
5. V. Rinnerbauer, Y.X. Yeng, W.R. Chan, J.J. Senkevich, J.D. Joannopoulos, M. Soljačić, I. Celanovic, Opt. Express **21**, 11482 (2013)
6. J.B. Chou, Y.X. Yeng, A. Lenert, V. Rinnerbauer, I. Celanovic, M. Soljačić, E.N. Wang, S.-G. Kim, Opt. Express **22**, A144 (2014)
7. B. Gesemann, S.L. Schweizer, R.B. Wehrspohn, Photonic. Nano. Fund. Appl. **8**, 107 (2010)
8. S. Han, B.J. Lee, Int. J. Heat Mass Transfer. **84**, 713 (2015)
9. A. Kohiyama, M. Shimizu, H. Kobayashi, F. Iguchi, H. Yugami, Energy Proc. **57**, 517 (2014)
10. B. Zhao, L. Wang, Y. Shuai, Z.M. Zhang, Int. J. Heat Mass Transfer. **67**, 637 (2013)
11. Y.S. Touloukian, D.P. DeWitt,: Thermal radiative properties: metallic elements and alloys (Springer US, Berlin, 2014)
12. Y.X. Yeng, W.R. Chan, V. Rinnerbauer, V. Stelmakh, J.J. Senkevich, J.D. Joannopoulos, M. Soljacic, I. Čelanović, Opt. Express **23**, A157 (2015)
13. Z. Zhou, E. Sakr, Y. Sun, and P. Bermel, Nanophotonics. **5**, 1 (2016)
14. T. Bauer, Thermophotovoltaics: basic principles and critical aspects of system design (Springer Science & Business Media, New York, 2011)
15. W.R. Chan, P. Bermel, R.C. Pilawa-Podgurski, C.H. Marton, K.F. Jensen, J.J. Senkevich, J.D. Joannopoulos, M. Soljačić, I. Celanovic, Proc. Natl. Acad. Sci. USA **110**, 5309 (2013)
16. R. Kivaisi, L. Stensland, Appl. Phys. A **27**, 233 (1982)
17. N. Nguyen-Huu, J. Pištora, M. Cada, Nanotechnology **27**, 155402 (2016)
18. Y.X. Yeng, W.R. Chan, V. Rinnerbauer, J.D. Joannopoulos, M. Soljačić, I. Celanovic, Opt. Express **21**, A1035 (2013)
19. Y. Nam, Y.X. Yeng, A. Lenert, P. Bermel, I. Celanovic, M. Soljačić, E.N. Wang, Sol. Energy Mat. Sol. Cells **122**, 287 (2014)
20. H. Sai, H. Yugami, Y. Akiyama, Y. Kanamori, K. Hane, J. Opt. Soc. Am. A **18**, 1471 (2001)
21. V. Rinnerbauer, A. Lenert, D.M. Bierman, Y.X. Yeng, W.R. Chan, R.D. Geil, J.J. Senkevich, J.D. Joannopoulos, E.N. Wang, M. Soljačić, Adv. Energy Mater. **4**, (2014)
22. Z. Zhou, Q. Chen, P. Bermel, Energy Convers. Manag. **97**, 63 (2015)
23. J.-Y. Chang, Y. Yang, L. Wang, Int. J. Heat Mass Transfer. **87**, 237 (2015)
24. D. Chubb, Fundamentals of thermophotovoltaic energy conversion (Elsevier, Amsterdam, 2007)
25. H. Ye, H. Wang, Q. Cai, J. Quant. Spectrosc. Radiat. Transfer. **158**, 119 (2015)
26. V. Stelmakh, V. Rinnerbauer, R. Geil, P. Aimone, J. Senkevich, J. Joannopoulos, M. Soljačić, I. Celanovic, Appl. Phys. Lett. **103**, 123903 (2013)
27. I. Celanovic, N. Jovanovic, J. Kassakian, Appl. Phys. Lett. **92**, 193101 (2008)
28. Y.-B. Chen, Z. Zhang, Opt. Commun. **269**, 411 (2007)
29. H. Sai, H. Yugami, Appl. Phys. Lett. **85**, 3399 (2004)
30. H. Sai, Y. Kanamori, K. Hane, H. Yugami, J. Opt. Soc. Am. A **22**, 1805 (2005)
31. S. Lin, J. Fleming, Z. Li, I. El-Kady, R. Biswas, K.M. Ho, J. Opt. Soc. Am. B. **20**, 1538 (2003)
32. H. Sai, Y. Kanamori, H. Yugami, J. Micromech. Microeng. **15**, S243 (2005)
33. H. Sai, Y. Kanamori, H. Yugami, Appl. Phys. Lett. **82**, 1685 (2003)
34. A. Taflove, A. Oskooi, and S.G. Johnson, Advances in FDTD computational electrodynamics: photonics and nanotechnology (Artech house, Norwood, 2013)
35. A.F. Oskooi, D. Roundy, M. Ibanescu, P. Bermel, J.D. Joannopoulos, S.G. Johnson, Comput. Phys. Commun. **181**, 687 (2010)
36. A.D. Rakić, A.B. Djurišić, J.M. Elazar, and M.L. Majewski, Appl. opt. **37**, 5271 (1998)
37. D. Chester, P. Bermel, J.D. Joannopoulos, M. Soljacic, I. Celanovic, Opt. Express. **19**, A245 (2011)
38. I. Celanovic, D. Perreault, J. Kassakian, Phys. Rev. B. **72**, 075127 (2005)
39. H. Sai, Y. Kanamori, Microscale. Thermophys. Eng. **7**, 101 (2003)
40. M. Shimizu, H. Yugami, J. Therm. Scie. Tech. **6**, 297 (2011)
41. D. Smith, W. Daenner, Y. Gohar, (ITER blanket, shield and material data base International Atomic Energy Agency, Vienna, 1991)
42. R. Knibbs, J. Phys. E **2**, 515 (1969)
43. J. Jackson, J.D. Jackson, Wie classical electrodynamics, 3rd edn. (John Wiley & Sons, Limited, 2005)
44. M. Ghebrebrhan, P. Bermel, Y. Yeng, I. Celanovic, M. Soljačić, J. Joannopoulos, Phys. Rev. A **83**, 033810 (2011)
45. R. Gordon, A.G. Brolo, Opt. Express **13**, 1933 (2005)
46. E. Lansey, N. Pishbin, J.N. Gollub, D.T. Crouse, J. Opt. Soc. Am. B **29**, 262 (2012)
47. H. Shin, P.B. Catrysse, S. Fan, Phys. Rev. B **72**, 085436 (2005)
48. F. Kusunoki, J. Takahara, T. Kobayashi, Electron. Lett. **39**, 23 (2003)
49. D. Peykov, Y.X. Yeng, I. Celanovic, J.D. Joannopoulos, and C. A. Schuh, Opt. Express **23**, 9979 (2015)